Surface changes on comet 67P/Churyumov-Gerasimenko suggest a more active past

Authors: M. Ramy El-Maarry[1,2*], O. Groussin[3], N. Thomas[1], M. Pajola[4], A.-T. Auger[3], B. Davidsson[5], X. Hu[6], S. F. Hviid[7], J. Knollenberg[7], C. Güttler[6], C. Tubiana[6], S. Fornasier[8], C. Feller[8], P. Hasselmann[8], J.-B. Vincent[7], H. Sierks[6], C. Barbieri[9], P. Lamy[10], R. Rodrigo[11,12], D. Koschny[13], H. U. Keller[7,14], H. Rickman[15,16], M. F. A'Hearn[17], M. A. Barucci[8], J.-L. Bertaux[18], I. Bertini[9], S. Besse[13], D. Bodewits[17], G. Cremonese[19], V. Da Deppo[20], S. Debei[21], M. De Cecco[22], J. Deller[6], J. D. P. Deshapriya[8], M. Fulle[23], P. J. Gutierrez[24], M. Hofmann[6], W.-H. Ip[25], L. Jorda[3], G. Kovacs[6], J.-R. Kramm[6], E. Kührt[7], M. Küppers[13], L. M. Lara[24], M. Lazzarin[9], Z.-Yi Lin[25], J. J. Lopez Moreno[24], S. Marchi[26], F. Marzari[9], S. Mottola[7], G. Naletto[27,28,20], N. Oklay[6], A. Pommerol[1], F. Preusker[7], F. Scholten[7], X. Shi[6]

Affiliations:

[1]Physikalisches Institut, Universität Bern, Sidlerstrasse 5, 3012 Berne, Switzerland.

[2]Laboratory for Atmospheric and Space Physics, University of Colorado, 3665 Discovery Drive, CO 80301, USA.

[3]Aix Marseille Université, CNRS, LAM (Laboratoire d'Astrophysique de Marseille), UMR 7326, 13388 Marseille, France.

[4]NASA Ames Research Center, Moffett Field, CA 94035, USA.

[5]Jet Propulsion Laboratory, 4800 Oak Grove Drive, Pasadena, CA 91109, USA.

[6]Max-Planck-Institut für Sonnensystemforschung, Justus-von-Liebig-Weg 3, 37077 Göttingen, Germany.

[7]Deutsches Zentrum für Luft- und Raumfahrt (DLR), Institut für Planetenforschung, Rutherfordstraße 2, 12489 Berlin, Germany.

[8]LESIA, Observatoire de Paris, PSL Research University, CNRS, Univ. Paris Diderot, Sorbonne Paris Cité, UPMC Univ. Paris 06, Sorbonne Universités, 5 Place J. Janssen, Meudon Principal Cedex 92195, France.

[9]Department of Physics and Astronomy, University of Padova, Vicolo dell'Osservatorio 3, 35122 Padova, Italy.

[10]Laboratoire d'Astrophysique de Marseille, UMR 7326 CNRS and Université Aix-Marseille, 38 rue Frédéric Joliot-Curie, 13388 Marseille Cedex 13, France.

[11]Centro de Astrobiología, CSIC-INTA, 28850 Torrejón de Ardoz, Madrid, Spain.

[12]International Space Science Institute, Hallerstraße 6, 3012 Berne, Switzerland.

[13]Operations Department, European Space Astronomy Centre/ESA, P.O. Box 78, 28691 Villanueva de la Cañada, Madrid, Spain.

[14]Institut für Geophysik und extraterrestrische Physik (IGEP), Technische Universität Braunschweig, Mendelssohnstr. 3, 38106 Braunschweig, Germany.

[15]Department of Physics and Astronomy, Uppsala University, Box 516, 75120 Uppsala, Sweden.

[16]PAS Space Research Center, Bartycka 18A, 00716 Warsaw, Poland.

[17]Department of Astronomy, University of Maryland, College Park, MD 20742-2421, USA.

[18]LATMOS, CNRS/UVSQ/IPSL, 11 Boulevard d'Alembert, 78280 Guyancourt, France.

[19]INAF, Osservatorio Astronomico di Padova, Vicolo dell'Osservatorio 5, 35122 Padova, Italy.

[20]CNR-IFN UOS Padova LUXOR, Via Trasea, 7, 35131 Padova, Italy.

[21]Department of Industrial Engineering, University of Padova, Via Venezia, 1, 35131 Padova, Italy.

[22]University of Trento, via Sommarive, 9, 38123 Trento, Italy.

[23]INAF, Osservatorio Astronomico di Trieste, Via Tiepolo 11, 34014 Trieste, Italy.

[24]Instituto de Astrofísica de Andalucía (CSIC), c/ Glorieta de la Astronomía s/n, 18008 Granada, Spain.

[25]Graduate Institute of Astronomy, National Central University, 300 Chung-Da Rd, Chung-Li 32054, Taiwan.

[26]Solar System Exploration Research, Virtual Institute, Southwest Research Institute, 1050 Walnut St., Suite 300, Boulder, CO 80302, USA.

[27]Department of Information Engineering, University of Padova, Via Gradenigo 6/B, 35131 Padova, Italy.

[28]Centro di Ateneo di Studi ed Attivitá Spaziali "Giuseppe Colombo" (CISAS), University of Padova, Via Venezia 15, 35131 Padova, Italy.

*Correspondence to: (mohamed.elmaarry@lasp.colorado.edu).

Abstract: The Rosetta mission spent nearly two years orbiting comet 67P/Churyumov-Gerasimenko mostly at distances that allow surface characterization and monitoring at sub-meter scales. During the Dec 2014–Jun 2016 period, numerous remarkable, yet localized, changes were observed, which we attribute to cometary-specific weathering, erosion, and unique transient events driven by insolation and other processes. While the localized changes suggest compositional or physical heterogeneity, their scale has not resulted in significant alterations to the comet's landscape. This suggests that most of the major landforms were created early in the comet current orbital configuration, or earlier if the comet had a larger volatile inventory, particularly of CO/CO_2 ices, or contained amorphous ice, which could trigger activity at larger distances from the Sun.

One Sentence Summary: Comets' surfaces change on seasonal scales, displaying evidence for weathering, intensive localized erosion, and unique short-scale morphological changes.

Main Text:

The ability to map the surface of a comet at sub-meter resolution, and closely monitor it through its journey in the inner solar system, were two key goals for the Rosetta mission to comet 67P/Churyumov-Gerasimenko (hereinafter referred to as 67P). The initial characterization of the surface upon arrival in Aug 2014 (*1*) showed 67P's surface to be diverse in its morphology, comprising different surface textures, which included rough consolidated terrains, smooth plains, unconsolidated mantles, and ubiquitous boulders (e.g., *2*–*5*). Following perihelion (Aug 13, 2015), we carried out a comparative analysis of many regions of the comet's northern hemisphere and equatorial regions to look for morphological or physical changes (*6*). Here, we present the most significant events we observed using the Optical, Spectroscopic, and Infrared Remote Imaging System (OSIRIS, *7*).

Erosion (text S1) on the surface of the comet appears to begin as in-situ weathering of consolidated surfaces, which acts to weaken these materials causing their fragmentation. This effect is evident in two locations where cliff collapses have taken place in the Seth (Fig. 1A, see Fig. S1 for regional definitions) and Ash regions (Fig. S2). The collapsing material detached at the locations of pre-existing fractures 10s of meters-long. Fractures play a significant role in driving cliff failures on Earth (e.g. *9*). On 67P, the failures were probably initiated by insolation weathering as a fracturing process (10), and triggered by associated, or proximal activity (*11*).

In the neck region, a large pre-existing >500 m-long fracture running through the northern neck has extended for at least 30 m (Figs. 1B, S3), along with development of new fractures parallel to it. The morphology and setting of these fractures is consistent with tensile fractures (*10*,*12*), particularly the lack of additional splitting at the fracture tips (*12*). The earliest extension of the fracture was detected in Dec. 2014 images (Fig. S3). 67P's spin rate increased steadily from Oct. 2014 to a maximum in late May 2015 (*13*,*14*) as a result of activity-induced torques (*13*). Recent finite-element models (*12*) suggest that increases in the spin rate could lead to development of tensile stresses in the neck region, which would lead to extension of pre-existing fractures and development of new ones, consistent with our observations. However, the presence of other lineaments with differing orientations (Fig. 1B) suggests possible evolution of the stress regime with time.

In the southern/near-equatorial Khonsu region a 20x30x40 m-wide boulder has moved a distance of ~140 m (Fig. 1C) around perihelion (Fig. S4). The resulting volume of ~24,000 m^3 corresponds to a mass of 12.8 x 10^6 kg assuming bulk density of 533 kg/m^3 (*15*), which would be comparable to lifting a ~450 kg boulder on Earth. Images taken shortly before and after perihelion (Fig. S5) show multiple outburst events (intensive and localized jet activity) close to the boulder's position, which could likely be responsible for the movement of the boulder. Viable processes are erosion of the sloped surface where the boulder resided, thus leading to its rolling downslope, or direct uplift if the outburst was strong enough, i.e. having a flux exceeding 25 kg s^{-1} (text S2).

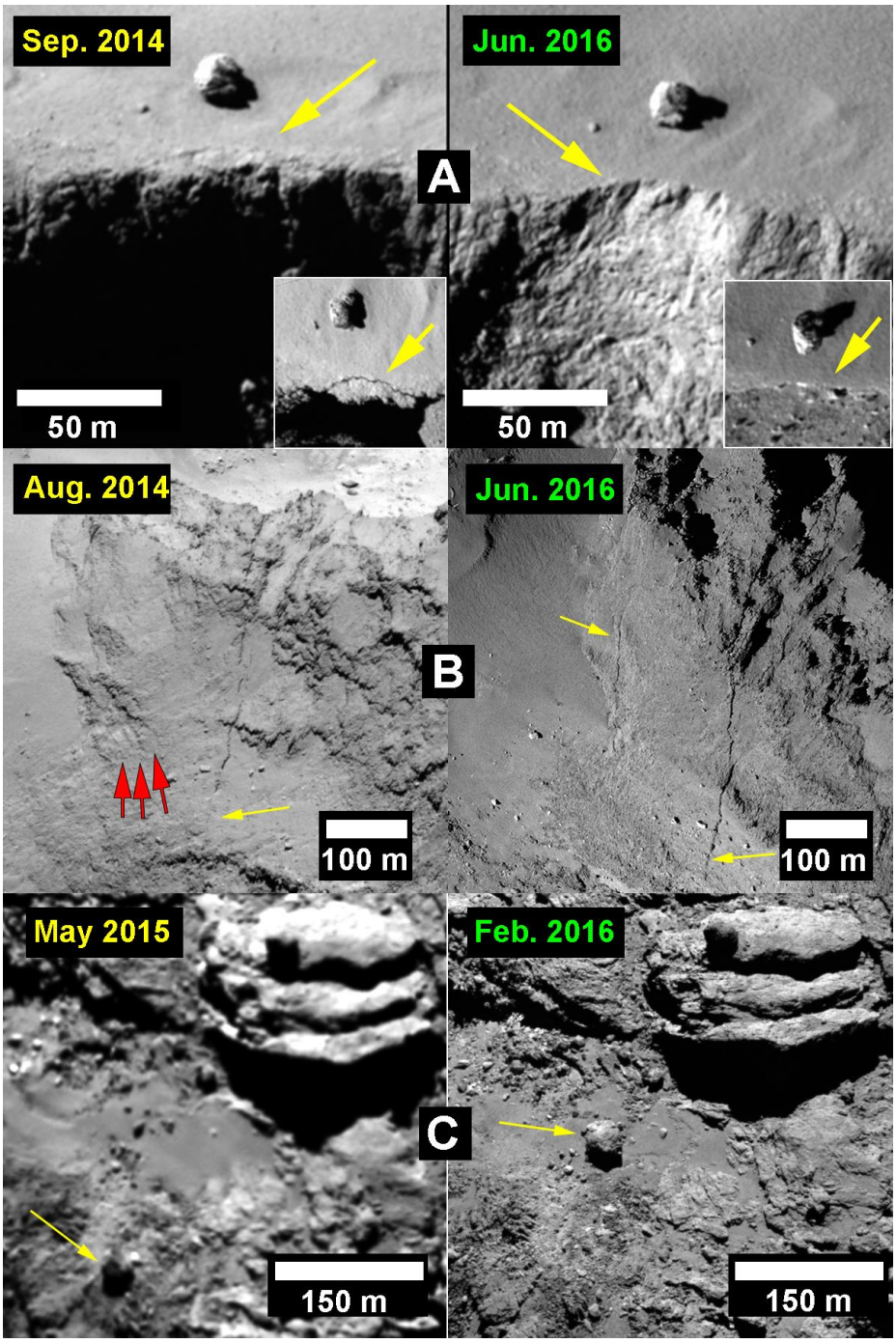

Fig. 1. Weathering-related changes on 67P. Panel A shows a cliff collapse on the large lobe in a location dubbed "Aswan" (*8*). The detached segment was ~12 m-wide whereas the fracture was ~50 m-long (*8*). Panel B shows an extension of a pre-existing fracture in the neck region in addition to the development of a new one parallel to it. Note the multiple lineaments with variable orientations (red arrows). Panel C shows a large boulder that has moved for a distance of ~140 m in the Khonsu region. In all panels, the yellow arrows point to the features of interest. Throughout the paper, the dates shown are the approximate acquisition time of the images. Their color indicates whether the image was acquired before (yellow) or after (green) perihelion. Additional details are in Table S1.

In addition to in-situ weathering, we have observed probable indicators of erosional transport of unconsolidated materials on the surface of 67P, resulting in the exhumation of previously covered surfaces. For instance, the Imhotep region shows a diverse surface characterized by smooth terrains and unique circular structures (*4*). One particular location in this region has been substantially exhumed to reveal previously covered circular features and small boulders (Fig. 2). Using an image acquired at a distance of ~6 km from the surface (corresponding to a resolution of 0.11 m/pixel, Fig. 2C), we calculate the height of the exhumed section of a boulder to be $3.9^{+0.1}_{-0.2}$ SD m. The errors correspond to inherent uncertainties in the Spacecraft and Planet Kernels (SPK). We have also discarded the highest point of the boulder (Fig. 2C), which was originally exposed, from our measurements. This estimate indicates that the extent of vertical erosion at this particular location exceeded 3 m.

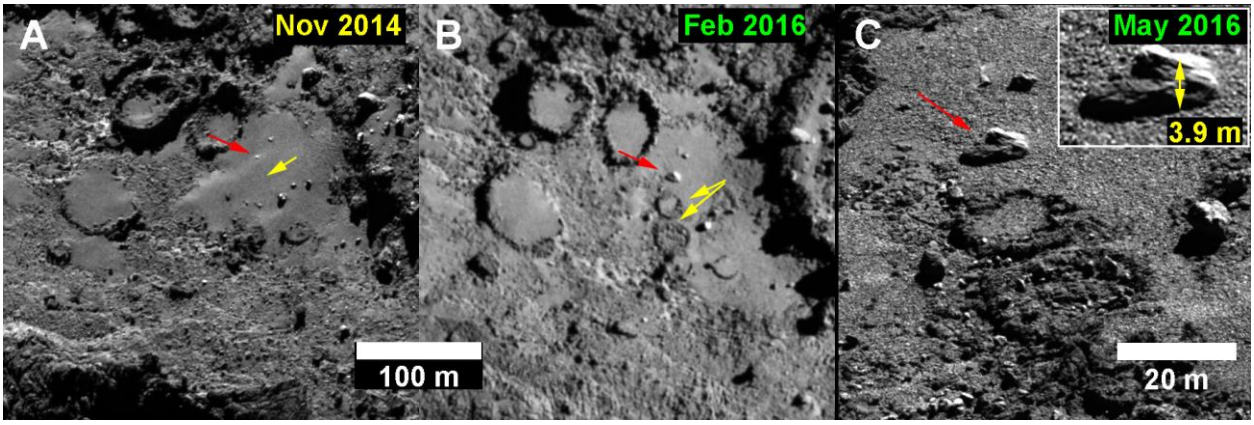

Fig. 2. Evidence of erosion in the Imhotep region. In all panels the direction of sunlight is from the upper right corner. Panel A: An image taken in Nov. 2014 shows a number of circular features and a blanket of smooth materials almost completely covering a number of boulders (note the one marked by a red arrow). The yellow arrow marks the location of two circular features exposed in later figures. Panel B: Two new circular features appear in this image taken in Feb. 2016. Note the exhumation of the boulder as well. Panel C: A higher-resolution image showing the two circular features, and the large boulder (inbox).

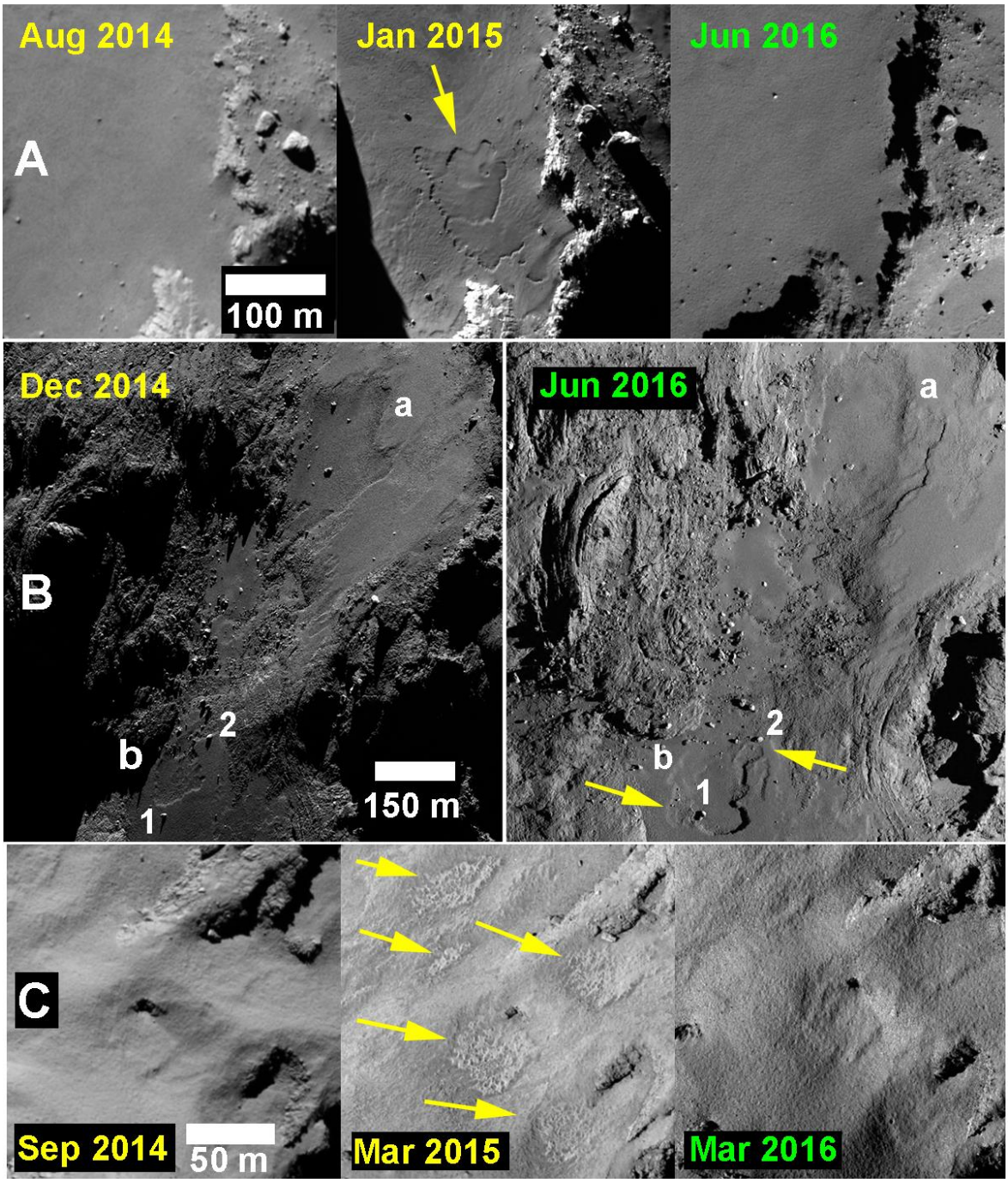

Fig. 3. Transient surface changes on 67P. Panel A: A view of a particular location in the Hapi region (the northern neck) that appeared smooth and featureless in Aug. 2014, then displayed pit-and-scarp patterns early in 2015, which had completely disappeared by the time the area was re-imaged after perihelion. Panel B: Distinctive morphological changes characterized by scarp retreat were also observed in the Anubis region particularly in areas "a" and "b" (see Fig S6). Area "b" in particular shows a retreat of the scarp in post perihelion bypassing a boulder (marked "1") and reaching another boulder "2" on the opposite side. Panel C: An area in the Ma'at region on the small lobe shows a smooth surface that undergoes transient changes as the comet approaches perihelion creating "honeycomb" structures.

Another set of observations shows unique morphological changes that directly affect the unconsolidated materials. These changes are mainly transient since they appear to gradually fade away with time as the surface almost reverts to its original appearance. In the smooth terrains such as Hapi (Fig. 3A), Anubis (Fig 3B), and Imhotep (*16*, Fig. S6), the changes are marked by the appearance and/or receding of shallow scarps (~1–5 m-deep from shadow measurements, text S3) forming quasi-circular or pitted patterns, which may enlarge with time, and later stop their evolution (e.g., Anubis) or gradually fade away (e.g., Hapi). During their evolution, the scarps may display brightening (e.g., Fig. S7), indicative of exposed water ice using spectrophotometric analysis (*17*, text S4, Fig. S8). A near-continuous time series of images around perihelion for the Anubis region indicates an average rate of scarp retreat of ~5.4 m/day at feature "a" (Fig. 3B and S7) close to perihelion, which is consistent with a similar range of values (4.3–7.6 m/day) observed at Imhotep (*16*). In total, features "a" and "b" displayed scarp retreats of ~35 m and ~50 m, respectively (text S5). These values are markedly higher than similar changes at comet 9P/Tempel 1 (~25 m/orbit) [*18*], which could be attributed to a smaller perihelion distance for 67P (1.3 au vs 1.5 au for 9P).

Early in the mission, (*2*) noted the presence of eolian-like ripple formations in the Hapi region. Close monitoring of these features showed that this location became a nucleus for the development of similar growing circular features by scarp retreat with associated brightening (Fig. S9) reaching a diameter ~100 m in less than 3 months, which in time faded away and created a new set of ripples. Recent models (*19*) predict that activity in the neck would generate high outgassing speeds (~500 m/s). These gases would then get funneled over the ripples area, and perpendicular to their long axes, mainly due to the comet's irregular shape (*19*), which may explain the recurring nature of the ripples. Similarly in the Imhotep region, we observed similar circular transient circular features (Fig. S10) on the smooth materials previously overlying the now exhumed terrain (Fig. 2). Therefore, we can infer that the development of transient roundish patterns, coupled with brightening, is an indicator of materials being actively eroded.

Finally, starting in Mar. 2015, numerous patches on the surface of dust-covered terrains (*2,3*), particularly in the Ma'at region (Fig. 3C) underwent textural changes marked by increase in surface roughness to form "honeycomb"-like features (*20*). Similar to other seasonal changes, these features have faded substantially in post-perihelion images. The fading has occurred probably due to resurfacing through deposition of new particles likely ejected from the southern hemisphere during intensive perihelion activity (*21*).

The significant, yet localized, changes in the comet mainly occur around perihelion (Fig. 4A). Many of the changes (e.g., boulder movement [Fig. 1C], erosion in Imhotep [Fig. 2], and transient changes [Fig. 3]) appear to be driven by insolation as they take place close to the corresponding sub-solar latitude (SSL, Fig. 4B), but there are notable exceptions, particularly the fracture extension in the neck (Fig. 1B), which is related to the comet's spin rate, pit-and-scarp patterns in the Hapi region (Fig 3A), and the cliff collapses (Figs. 1A, S1). The changes in Hapi can be attributed to the peculiar geometry of the northern neck leading to significant self-heating and earlier onset of activity (*21*). The collapsing cliffs are a special case because they receive more solar input when the vertical walls are illuminated compared to the time when the Sun is illuminating from the top (i.e. when corresponding to the SSL). Regardless, they occur around perihelion time at distances < 2 au, like most of the observed changes. Finally, the deviation of the changes in Anubis from the SSL could be a result of the SSL's rapid shift in perihelion (Fig. 4B), and therefore an observation bias.

The changes in the smooth terrains are remarkably constrained to the same latitude range (~10S) but appear as a chain of events rather than simultaneously. This could either indicate different thermo-physical surface properties or geometrical influences. Particularly, self-heating would trigger earlier activity in Hapi as discussed above. In turn, Imhotep is relatively flat and is exposed to sunlight over a wider range of incidence angles than the smooth plains of Anubis, which are enclosed by higher elevated regions, therefore becoming active later. Nevertheless, the highly localized nature of all the observed changes suggests compositional and or physical heterogeneity on the comet's surface at the scale of the observed changes (i.e., 10s of meters).

It is also important to note that no major changes to the comet's landscape have occurred that have significantly altered its shape or major landforms, even in the southern hemisphere where lower resolution, yet adequate data is available from May 2015. Given that the comet has only spent <10 orbits in its current close configuration since 1959 (e.g., *22*), it it is possible that earlier perihelion passages were significantly more active than what Rosetta witnessed to account for the higher needed rates of change. However, ground-based observations suggest similar levels of activity in previous orbits, though only as far back as 1982 (*23*). Alternatively, the comet's landscape may have evolved to its current form at a different time of the comet's lifetime possibly during its 1840 orbital configuration when 67P had a perihelion distance of 2.74 au (*22*). This distance would still lead to active modification of the surface (Fig. 4) but would require more vigorous activity, which could be possible if CO/CO_2 sublimation was involved (due to its sublimation at lower temperatures and consequently activity at larger distances), and the comet had a higher inventory of it in the past. In addition, crystallization of amorphous ice could have triggered higher rates of activity at earlier epochs when comet 67P was in its centaur phase (e.g., *24*,*25*) due to the exothermic nature of transition from amorphous to crystalline ice.

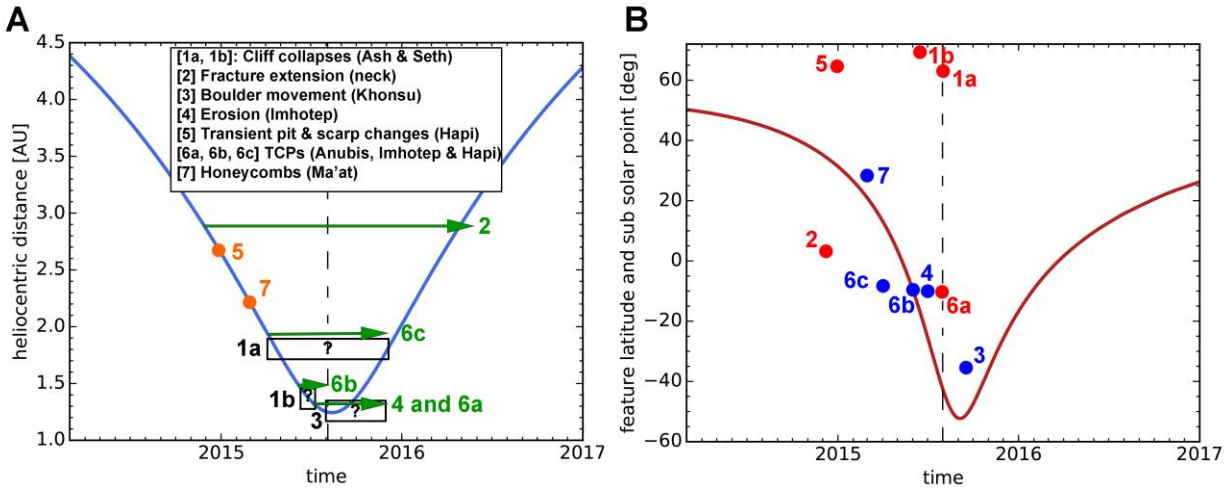

Fig. 4. Summary of event timeline versus heliocentric distance (A) and sub solar latitude [SSL] (B). The dashed line points to perihelion period. In panel A, TCPs in the legend stands for "transient circular patterns". Orange colors represent single events of confirmed time, green arrows represent continuous activity in a given period, and black boxes represent single events where the exact time is unknown but constrained to a given period. In panel B: blue dots signify events that appear to be insolation-driven, i.e., active within ±20º of the SSL. Red dots represent events that appear to be driven by other processes. Additional information is in table S2.

References and Notes:

1. Sierks, H. et al. Science **347** (2015). DOI: 10.1126/science.aaa1044
2. Thomas, N. *et al*. Science **347,** (2015). DOI: 10.1126/science.aaa0440.
3. El-Maarry, M. R. *et al.* Astronomy & Astrophysics **583**, A-26 (2015).
4. Auger, A-T. *et al*. Astronomy & Astrophysics **583**, A-35 (2015).
5. Pajola, M. *et al*. Astronomy & Astrophysics **583**, A-37 (2015).
6. See Materials and Methods in the online supplementary material.
7. Keller, H. U. *et al.* Space Sci. Rev. **128**, 433–506 (2007).
8. Pajola, M. *et al*. Astronomy & Astrophysics **592,** A-69 (2016).
9. Duperret, A., Genter, A., Martinez, A., Mortimore, R. N. Geo. Soc., London, Eng. Geo. Spec. Pub. **20**, 33–55, (2004).
10. El-Maarry, M. R. *et al.* Geophys. Res. Lett. **42,** 5170–5178 (2015).
11. Vincent, J. -B. *et al.* Astronomy & Astrophysics **587,** A-14 (2016).
12. Hirabayashi, M. *et al.* Nature **534**, doi:10.1038/nature17670 (2016).
13. Keller, H. U., Mottola, S., Skorov, Y. & Jorda, L. Astronomy & Astrophysics **579,** L-5 (2015).
14. Jorda, L. *et al.* Icarus 277, 257–278 (2016).
15. Pätzold, M. *et al.* Nature **530**, 63–65 (2016).
16. Groussin, O. *et al.* Astronomy & Astrophysics **583**, A-36 (2015).
17. Fornasier, S. *et al*. Science, doi: 10.1126/science.aag2671.
18. Thomas, P. *et al*. Icarus **222**, 453–466 (2013).
19. Thomas, N. *et al*. Astronomy & Astrophysics **583**, A-17 (2015).
20. Shi, X. *et al*. Astronomy & Astrophysics **586,** A-7 (2016).
21. Keller, H. U. *et al.* Astronomy & Astrophysics **583,** A-34 (2015).
22. Belyaev, N., Kresak, L., Pittich. E. M. Slovak Academy of Sciences, Astronomical Institute, Bratislava (1986).
23. Snodgrass, C. *et al*. Astronomy & Astrophysics. **588,** A-80 (2016).
24. Jewitt, D. Astronom. J. **137**, 4296–4312, (2009).
25. Prialnik, D and Bar-Nun, A. Astrophys. J., **313**, 893–905, (1987).
26. Tubiana, C. *et al.*, Astronomy & Astrophysics **583,** A-46 (2015).
27. Gombosi, T.I., Nagy, A. F., Cravens, T. E. Rev. Geophys. **24**, 667–700 (1986).
28. Fulle, M. Astronomy & Astrophysics **325**, 1237–1248 (1997).
29. Crifo, J. F. Astronomy & Astrophysics **223**, 365–368, (1989).
30. Bailey, A. B., Hiatt, J. Amer. Inst. Aeronautics & Astronautics J. **10**, 1436–1440, (1972).

Acknowledgments: OSIRIS was built by a consortium of the Max-Planck-Institut für Sonnensystemforschung, in Göttingen, Germany; Centro Interdipartimentale di Studi e Attività Spaziali–University of Padova, Italy; the Laboratoire d'Astrophysique de Marseille, France; the Instituto de Astrofísica de Andalucia, Consejo Superior de Investigaciones Cientificas, Granada, Spain; the Research and Scientific Support Department of the European Space Agency (ESA), Noordwijk, Netherlands; the Instituto Nacional de Técnica Aeroespacial, Madrid, Spain; the Universidad Politećhnica de Madrid, Spain; the Department of Physics and Astronomy of Uppsala University, Sweden; and the Institut für Datentechnik und Kommunikationsnetze der Technischen Universität Braunschweig, Germany. The support of the national funding agencies of Germany (Deutschen Zentrums für Luft- und Raumfahrt), France (Centre National

d’Etudes Spatiales), Italy (Agenzia Spaziale Italiana), Spain (Ministerio de Educación, Cultura y Deporte), Sweden (Swedish National Space Board; grant no. 74/10:2), and the ESA Technical Directorate is gratefully acknowledged. H.R. was also supported bygrant no. 2011/01/B/ST9/05442 of the Polish National Science Center. W.-H.I acknowledges the Ministry of Science and Technology, Taiwan (grant no. NSC 101-2111-M-008-016). M.F.A. acknowledges NASA funding through Jet Propulsion Laboratory contract no. 1267923. We thank the ESA teams at European Space Astronomy Centre, European Space Operations Centre, and European Space Research and Technology Centre for their work in support of the Rosetta mission. The data will be placed in ESA’s Planetary Sciences Archive after the proprietary period and are available on request until that time.

Supplementary Materials:

Materials and Methods

Supplementary text S1–S5

Figures S1–S10

Tables S1–S2

References 26–30